A cheap and easy-to-implement upwind scheme for second order traffic flow models

Alexandra Würth, Paola Goatin, Luis Miguel Villada

A cheap and easy-to-implement upwind scheme for second order traffic flow models

Alexandra Würth, Paola Goatin and Luis Miguel Villada

Abstract We extend the finite volume numerical scheme proposed by Hilliges and Weidlich [11] to second order traffic flow models consisting in 2×2 systems of non strictly hyperbolic conservation laws of Temple class. The scheme is shown to satisfy some maximum principle properties on the density. We provide numerical tests illustrating the behaviour at vacuum and the gain in computational time when dealing with optimization algorithms.

1 Introduction

The Generic Second Order Model [13] provides a general framework for macroscopic traffic flow modeling. In particular, it generalises the classical Lighthill-Whitham-Richards (LWR) model [14, 16] and includes the widely used Aw-Rascle-Zhang (ARZ) system [2, 19]. We recall that second order models are able to capture several traffic behaviours, such as stop-and-go waves and non-equilibrium regimes, in particular in congested situations. They can therefore be used for better traffic state reconstruction and prediction [18], for which efficient numerical simulations are of utmost importance. For this, most of the literature relies on a supply-demand formulation of Godunov scheme, see e.g [12], which allows for sharp approximations, but is quite cumbersome to code. A much easier and cheaper alternative is offered by an upwind type finite volume scheme proposed by [11] for the scalar case and more extensively studied in [4] for multi-class models.

Alexandra Würth and Paola Goatin
Université Côte d'Azur, Inria, CNRS, LJAD, Sophia Antipolis, France, e-mail: {alexandra.wuerth, paola.goatin}@inria.fr

Luis Miguel Villada
GIMNAP-Departamento de Matemáticas, Universidad del Bío-Bío, Concepción, Chile; CI^{2}MA-Universidad de Concepción, Casilla 160-C, Concepción, Chile, e-mail: lvillada@ubiobio.cl

In this paper, we prove that the scheme is positivity preserving and obeys a maximum principle under the hypothesis of a unique zero-speed density. We also provide some tests exploring the behaviour of solutions involving vacuum states, and evidence of the computational gain offered by the proposed scheme.

2 General Second Order Models

Generic Second Order traffic flow Models (GSOM) [13] consist in the 2×2 system of conservation laws

$$\begin{cases} \partial_t \rho + \partial_x(\rho v) = 0, \\ \partial_t(\rho w) + \partial_x(\rho w v) = 0, \end{cases} \qquad x \in \mathbb{R},\ t > 0, \tag{1}$$

where the average speed of vehicles is a function of the density $\rho = \rho(t,x)$ and a Lagrangian vehicle property $w = w(t,x)$, namely $v = \mathcal{V}(\rho, w)$ for some speed function $\mathcal{V}$ satisfying

$$\mathcal{V}(\rho, w) \geq 0, \quad \mathcal{V}(0, w) = w, \quad \mathcal{V}_w(\rho, w) > 0, \tag{2a}$$

$$2\mathcal{V}_\rho(\rho, w) + \rho \mathcal{V}_{\rho\rho}(\rho, w) < 0, \tag{2b}$$

$$\forall w \in [w_{min}, w_{max}] \quad \exists\, R(w) > 0 \quad \text{s.t.} \quad \mathcal{V}(R(w), w) = 0, \tag{2c}$$

on a domain Ω of the form $\Omega := \left\{(\rho, w) \in \mathbb{R}^2 \mid \rho \in [0, R(w_{max})], w \in [w_{min}, w_{max}]\right\}$ with $0 < w_{min} \leq w_{max}$ [8].

As in [5, 8], we observe that (2b) implies that $\rho \mapsto Q(\rho, w) := \rho \mathcal{V}(\rho, w)$ is strictly concave and $\mathcal{V}_\rho(\rho, w) < 0$ for $w > 0$, if $\mathcal{V}$ is a $\mathbf{C^2}$ function in ρ. We also remark that in (2c) we can have $R(w) = \mathbf{R}_{\max}$ for all $w \in [w_{min}, w_{max}]$.

System (1) is strictly hyperbolic for $\rho > 0$, with eigenvalues

$$\lambda_1(\rho, w) = \mathcal{V}(\rho, w) + \rho \mathcal{V}_\rho(\rho, w), \qquad \lambda_2(\rho, w) = \mathcal{V}(\rho, w).$$

The first characteristic field is genuinely non-linear and the second linearly degenerate [3, Definition 5.2]. The associated Riemann invariants are

$$z_1(\rho, w) = \mathcal{V}(\rho, w), \qquad z_2(\rho, w) = w.$$

Since shock and rarefaction curves of each family coincide, the system belongs to the Temple class [17]. Notice that, setting $\mathcal{V}(\rho, w) = w - p(\rho)$ for a suitable "pressure" function p, system (1) corresponds to the ARZ model [2, 19] and, taking $w = \bar{w}$ constant, we recover the classical LWR model [14, 16] with $v_e(\rho) = \mathcal{V}(\rho, \bar{w})$.

Due to the loss of strict hyperbolicity at vacuum, it is not possible to give a unique definition of the solutions of Riemann problems involving vacuum states, even enforcing entropy conditions. Different options are proposed and discussed in the literature, see e.g. [1, 7]. In particular, if the right (downstream) state belongs to the vacuum, the solution can either consist of a rarefaction wave to the vacuum, or a first family wave (shock or rarefaction) followed by a contact discontinuity. More details on the construction of solutions and an existence result for the corresponding Initial Boundary Value Problem can be found in [9].

3 Hilliges-Weidlich numerical scheme

The most widely used numerical scheme for traffic flow macroscopic simulations is the finite volume Godunov scheme [10] in its Cell Transmission Model (CTM) version [6], where the fluxes across interfaces are given by the minimum of the sending capacity of the upstream cell and the receiving capacity at the downstream one. Here we propose a much simpler to implement alternative, which we will refer to as *Hilliges-Weidlich (HW) scheme* [11].

Given a space step Δx and a time step Δt satisfying the CFL condition

$$\Delta t \left\{ \|\mathcal{V}(\rho, w)\|_{\mathbf{L}^\infty(\Omega)} + R(w_{max}) \left\| \mathcal{V}_\rho(\rho, w) \right\|_{\mathbf{L}^\infty(\Omega)} \right\} \leq \Delta x, \tag{3}$$

let $x_{j+1/2} = j\Delta x$, $j \in \mathbb{Z}$, be the cell interfaces, and $t^n = n\Delta t$, $n \in \mathbb{N}$, the time mesh. Denoting by $\mathbf{u} = (\rho, y)^T = (\rho, \rho w)^T$ the vector of the conservative variables (where we set $y = \rho w$), we construct a finite volume approximate solution of (1) of the form $\mathbf{u}^{\Delta x} = (\rho^{\Delta x}, y^{\Delta x})^T$ with $\rho^{\Delta x}(t, x) = \rho_j^n$ and $y^{\Delta x}(t, x) = y_j^n$ for $(t, x) \in C_j^n = [t^n, t^{n+1}[\times [x_{j-1/2}, x_{j+1/2}[$. To this end, we approximate the initial data with piecewise constant functions

$$\rho_j^0 = \tfrac{1}{\Delta x} \int_{x_{j-1/2}}^{x_{j+1/2}} \rho^0(x)\, dx, \quad y_j^0 = \tfrac{1}{\Delta x} \int_{x_{j-1/2}}^{x_{j+1/2}} y^0(x)\, dx, \qquad \forall j \in \mathbb{Z},$$

and we iterate in time according to the conservation formulas

$$\mathbf{u}_j^{n+1} = \mathbf{u}_j^n - \frac{\Delta t}{\Delta x} \left(\mathbf{F}_{j+1/2}^n - \mathbf{F}_{j-1/2}^n \right), \tag{4}$$

with $\mathbf{F}_{j+1/2}^n = (F_{j+1/2}^{\rho,n}, F_{j+1/2}^{y,n})^T$, where

$$F_{j+1/2}^{\rho,n} = \rho_j^n\, \mathcal{V}^+(\rho_{j+1}^n, w_{j+1}^n) \qquad \text{and} \qquad F_{j+1/2}^{y,n} = w_j^n\, F_{j+1/2}^{\rho,n} \tag{5}$$

are the flow respectively of ρ and y at $x = x_{j+1/2}$ in the time interval $[t^n, t^{n+1}[$, and we set $\mathcal{V}^+(\rho, w) := \max\{\mathcal{V}(\rho, w), 0\}$. Indeed, since contact discontinuity waves have positive speed and the variable w is advected with ρv, the choice (5) gives a good approximation of the flux at the interface, which corresponds to the Riemann problem given by $U_L = (\rho_j^n, w_j^n)$ and $U_M = (\rho_{j+1/2}^n, w_j^n)$. Here, U_M defines the intermediate state of the solution to the Riemann problem corresponding to U_L and $U_R = (\rho_{j+1}^n, w_{j+1}^n)$, where $\rho_{j+1/2}^n$ is implicitly defined by $\mathcal{V}(\rho_{j+1/2}^n, w_j^n) = \mathcal{V}(\rho_{j+1}^n, w_{j+1}^n)$, see Figure 1. Therefore we have

$$F_{j+1/2}^{\rho,n} = \rho_j^n\, \mathcal{V}^+(\rho_{j+1}^n, w_{j+1}^n) = \rho_j^n\, \mathcal{V}^+(\rho_{j+1/2}^n, w_j^n),$$

which reduces to the scalar case [4, 11].

Proposition 1 *Under the CFL condition* $\Delta t\, \|\mathcal{V}(\rho, w)\|_{\mathbf{L}^\infty(\Omega)} \leq \Delta x$, *which is weaker than* (3)*, the numerical scheme* (4)-(5) *is positivity preserving.*

Proof Let us assume that at time $t = t^n$, the approximate solution satisfies $\rho_j^n \geq 0$ for all $j \in \mathbb{Z}$. Then we get

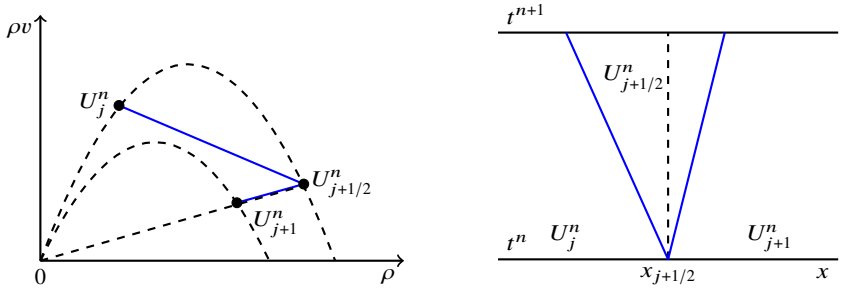

Fig. 1 Left: Phase-plane representation of an example of solution to the Riemann problem corresponding to $U_L = U_j^n = (\rho_j^n, w_j^n)$ and $U_R = U_{j+1}^n = (\rho_{j+1}^n, w_{j+1}^n)$, consisting of a shock joining U_L to $U_M = U_{j+1/2}^n = (\rho_{j+1/2}^n, w_j^n)$ and a contact discontinuity from U_M to U_R.
Right: Space-time representation of the Riemann solution at the corresponding cell interface.

$$\begin{aligned}\rho_j^{n+1} &= \rho_j^n - \frac{\Delta t}{\Delta x}\left(\rho_j^n \mathcal{V}^+(\rho_{j+1}^n, w_{j+1}^n) - \rho_{j-1}^n \mathcal{V}^+(\rho_j^n, w_j^n)\right)\\ &= \rho_j^n\left(1 - \frac{\Delta t}{\Delta x}\mathcal{V}^+(\rho_{j+1}^n, w_{j+1}^n)\right) + \frac{\Delta t}{\Delta x}\rho_{j-1}^n \mathcal{V}^+(\rho_j^n, w_j^n) \geq 0\end{aligned}$$

since $\Delta t\, \mathcal{V}^+(\rho_{j+1}^n, w_{j+1}^n) \leq \Delta x$ by assumption. □

Proposition 2 *Under the CFL condition* (3)*, if* $R(w) = \mathbf{R}_{max}$ *for all* $w \in [w_{min}, w_{max}]$*, the approximate solution constructed by* (4)-(5) *satisfies* $\rho_j^n \leq \mathbf{R}_{max}$ *for all* $j \in \mathbb{Z}$ *and* $n \in \mathbb{N}$*. In particular,* $\mathcal{V}(\rho_j^n, w_j^n) \geq 0$ *for all* $j \in \mathbb{Z}$ *and* $n \in \mathbb{N}$*.*

Proof We assume that at time $t = t^n$, the approximate solution satisfies $\rho_j^n \leq \mathbf{R}_{\max}$ for all $j \in \mathbb{Z}$. Then we get

$$\begin{aligned}\rho_j^{n+1} &= \rho_j^n - \frac{\Delta t}{\Delta x}\left[\rho_j^n \mathcal{V}^+(\rho_{j+1}^n, w_{j+1}^n) - \rho_{j-1}^n \mathcal{V}^+(\rho_j^n, w_j^n)\right]\\ &= \rho_j^n - \frac{\Delta t}{\Delta x}\left[\rho_j^n \mathcal{V}(\rho_{j+1/2}^n, w_j^n) - \rho_{j-1}^n \mathcal{V}(\rho_j^n, w_j^n)\right]\\ &= \rho_j^n - \frac{\Delta t}{\Delta x}\left[\rho_j^n \mathcal{V}(\rho_{j+1/2}^n, w_j^n) \pm \rho_j^n \mathcal{V}(\rho_j^n, w_j^n) - \rho_{j-1}^n \mathcal{V}(\rho_j^n, w_j^n)\right]\\ &= \rho_j^n - \frac{\Delta t}{\Delta x}\left[\rho_j^n \mathcal{V}_\rho(\xi_j^n, w_j^n)\left(\rho_{j+1/2}^n - \rho_j^n\right) + \mathcal{V}(\rho_j^n, w_j^n)\left(\rho_j^n - \rho_{j-1}^n\right)\right]\\ &= \rho_j^n\left[1 - \frac{\Delta t}{\Delta x}\left(b_j^n + a_j^n\right)\right] + \rho_{j+1/2}^n \frac{\Delta t}{\Delta x} b_j^n + \rho_{j-1}^n \frac{\Delta t}{\Delta x} a_j^n,\end{aligned}$$

for some $\xi_j^n \in [\min\{\rho_j^n, \rho_{j+1/2}^n\}, \max\{\rho_j^n, \rho_{j+1/2}^n\}]$ and setting $a_j^n := \mathcal{V}(\rho_j^n, w_j^n) \geq 0$ and $b_j^n := -\rho_j^n \mathcal{V}_\rho(\xi_j^n, w_j^n) \geq 0$ for all $j \in \mathbb{Z}$. Moreover, by (3), we get $1 - \frac{\Delta t}{\Delta x}(a_j^n + b_j^n) \geq 0$ and therefore we conclude

$$\rho_j^{n+1} \leq \mathbf{R}_{\max}\left[1 - \frac{\Delta t}{\Delta x}\left(b_j^n + a_j^n\right)\right] + \mathbf{R}_{\max}\frac{\Delta t}{\Delta x} b_j^n + \mathbf{R}_{\max}\frac{\Delta t}{\Delta x} a_j^n = \mathbf{R}_{\max}.$$ □

We remark that, in the general case, $R(w) \neq \mathbf{R}_{\max}$ for all $w \in [w_{min}, w_{max}]$, the positivity of the speed cannot be guaranteed. This is why we take $\mathcal{V}^+$ in (5).

4 Numerical tests

4.1 Riemann problems

In this section, we consider the Riemann problem for (1) with the ARZ speed function $\mathcal{V}(\rho, w) = w - p(\rho)$ with $p(\rho) = \rho$ and initial data of the form $(\rho, w)(0, x) = (\rho_L, w_L)$ if $x \leq 0.5$ and $(\rho, w)(0, x) = (\rho_R, w_R)$ if $x > 0.5$. We compare the solutions at $T = 0.5$ computed on the interval $[0, 1]$ by the Godunonv and HW schemes with absorbing boundary conditions. The numerical solutions are also compared with the entropy admissible analytical solutions proposed by [1] (denoted as Analitical Solution 1 - AS1) and [7] (AS 2).

4.1.1 Solutions involving vacuum states

Since the numerical scheme is expressed in conservative variables $(\rho, y = \rho w)$, the Lagrangian vehicle property w is not defined whenever $\rho = 0$. Thus, we demonstrate in this subsection that, whenever $\rho_j^n = 0$, setting $w_j^n = w_k^n$ with $k = \max_{i<j}\{i \colon \rho_i^n > 0\}$ (and $w_j^n = w_j^{n-1}$ if $j = 1$), is coherent with the density component of the Riemann solution stated in [9, Definition 1] in the cases involving vacuum states. Notice that, due to numerical viscosity, density at vacuum states may be not exactly zero, affecting the w and $v = \mathcal{V}(\rho, w)$ components.

In the following, we analyse the solution of the numerical solutions for different initial data.

- **Test 1:** middle vacuum state $\rho_M = 0$, see Figure 2. AS1 consists of a rarefaction from $U_L = (0.4, 0.5)$ to $(0, 0.5)$ followed by a contact discontinuity to $U_R = (0.1, 0.9)$ travelling with speed $\mathcal{V}(U_R) = 0.8$; AS2 is composed of a rarefaction wave connecting U_L to $(0, 0.5)$, followed by a vacuum wave and a contact discontinuity between $(0, 0.8)$ and U_R.
  While the ρ component is the same for all solutions, the w and v components of the numerical solutions match AS2, which is $\mathbf{L}^1$-stable in the Riemann invariants.
- **Test 2:** left vacuum state $\rho_L = 0$, see Figures 3 and 4.
  (A) Both analytical solutions are the juxtaposition of a shock from U_L to $(0.5, 0.7)$ and a contact discontinuity, moving at the same speed $\mathcal{V}(U_R) = 0.2$.
  (B) AS1 consists of a discontinuity between $U_L = (0, 0.4)$ and $U_R = (0.2, 0.8)$ travelling with speed $\mathcal{V}(U_R) = 0.6$; AS2 is a vacuum wave from U_L to $(0, 0.6)$ followed by a contact discontinuity.
  We observe that the numerical schemes capture the ρ component, but there is a discrepancy in the Riemann invariants: indeed, due to numerical viscosity, the

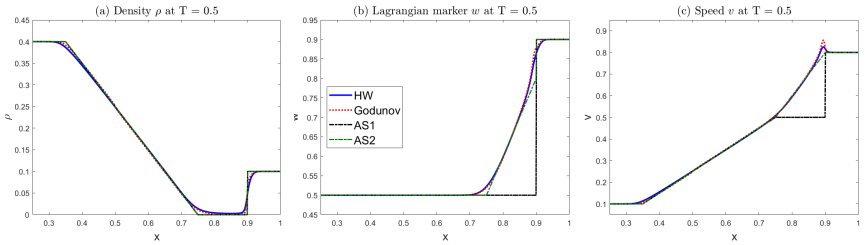

Fig. 2 Test 1. Solutions of the Riemann problem with $(\rho_L, w_L) = (0.4, 0.5)$, $(\rho_R, w_R) = (0.1, 0.9)$, computed by the Godunov and HW schemes at $T = 0.5$ with $\Delta x = \frac{1}{800}$, compared to the analytical solutions.

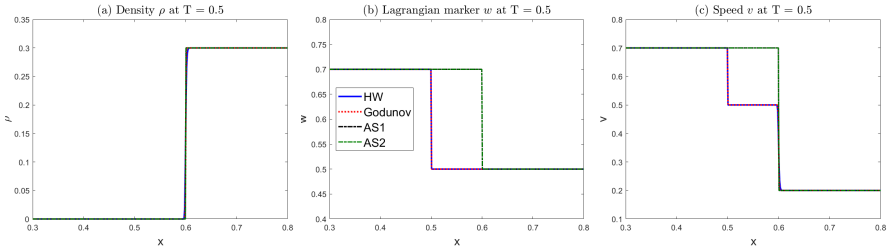

Fig. 3 Test 2 (A) Solutions of the Riemann problem with $(\rho_L, w_L) = (0, 0.7)$, $(\rho_R, w_R) = (0.3, 0.5)$, computed by the Godunov and HW schemes at $T = 0.5$ with $\Delta x = \frac{1}{800}$, compared to the analytical solutions.

approximate solutions consist of a stationary vacuum discontinuity followed by a shock from $(0, 0.5)$ (resp. $(0, 0.8)$) to U_R.

- **Test 3:** right vacuum state $\rho_R = 0$, see Figures 5, 6 and 7.
  (A) AS1 consists of a rarefaction wave from $U_L = (0.3, 0.5)$ to $(0, 0.5)$; in AS2, the rarefaction is followed by a vacuum wave from $(0, 0.5)$ to $(0, 0.7)$.
  (B) AS1 consists of a rarefaction wave from $U_L = (0.5, 0.7)$ to $(0, 0.7)$; AS2 is composed of a rarefaction from U_L to $(0.3, 0.7)$, followed by a contact discontinuity to $U_R = (0, 0.4)$ moving with speed $\mathcal{V}(U_R) = 0.4$.
  (C) AS1 consists of a rarefaction wave from $U_L = (0.3, 0.8)$ to $(0, 0.8)$; AS2 is composed of a shock from U_L to $(0.5, 0.8)$ with 0 speed, followed by a contact discontinuity to $U_R = (0, 0.3)$ moving with speed $\mathcal{V}(U_R) = 0.3$.
  In all the cases, the numerical solutions capture AS1 by construction.

4.1.2 Convergence order

To compare the performance of the numerical schemes, we consider the $\mathbf{L^1}$-error $\mathbf{L^1}(\Delta x)$ and the numerical order of accuracy $\gamma(\Delta x)$ for $\Delta x = \frac{1}{100}, \frac{1}{200}, \frac{1}{400}, \frac{1}{800}, \frac{1}{1600}$ at $t = T$, defined respectively by

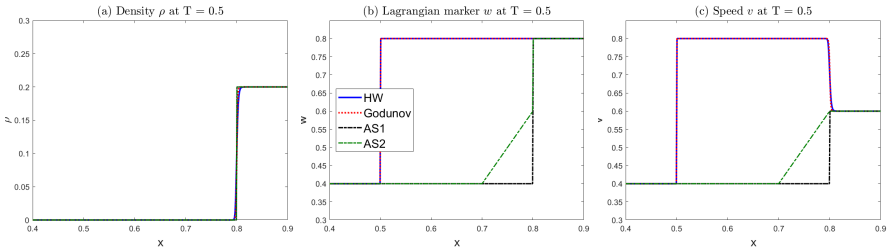

Fig. 4 Test 2 (B) Solutions of the Riemann problem with $(\rho_L, w_L) = (0, 0.4)$, $(\rho_R, w_R) = (0.2, 0.8)$, computed by the Godunov and HW schemes at $T = 0.5$ with $\Delta x = \frac{1}{800}$, compared to the analytical solutions.

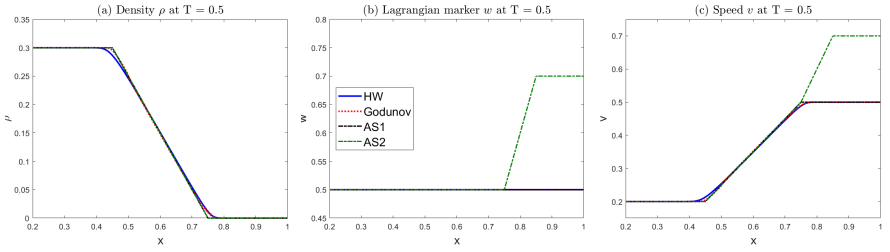

Fig. 5 Test 3 (A) Solutions of the Riemann problem with $(\rho_L, w_L) = (0.3, 0.5)$, $(\rho_R, w_R) = (0, 0.7)$, computed by the Godunov and HW schemes at $T = 0.5$ with $\Delta x = \frac{1}{800}$, compared to the analytical solutions.

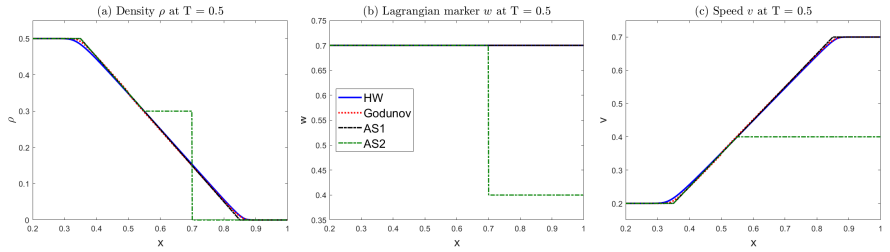

Fig. 6 Test 3 (B) Solutions of the Riemann problem with $(\rho_L, w_L) = (0.5, 0.7)$, $(\rho_R, w_R) = (0, 0.4)$, computed by the Godunov and HW schemes at $T = 0.5$ with $\Delta x = \frac{1}{800}$, compared to the analytical solutions.

$$\mathbf{L^1}(\Delta x) = \frac{1}{M}\sum_{j=1}^{M}\left\{|\rho_j^{\frac{T}{\Delta t}} - \bar{\rho}| + |y_j^{\frac{T}{\Delta t}} - \bar{y}|\right\}, \qquad \gamma(\Delta x) = \log_2\left(\frac{\mathbf{L^1}(2\Delta x)}{\mathbf{L^1}(\Delta x)}\right),$$

where $\bar{\rho}$ and $\bar{y}$ denote the cell averages of the exact Riemann solution at $t = T$ and M is the number of cells (see Table 1).

We consider two cases:

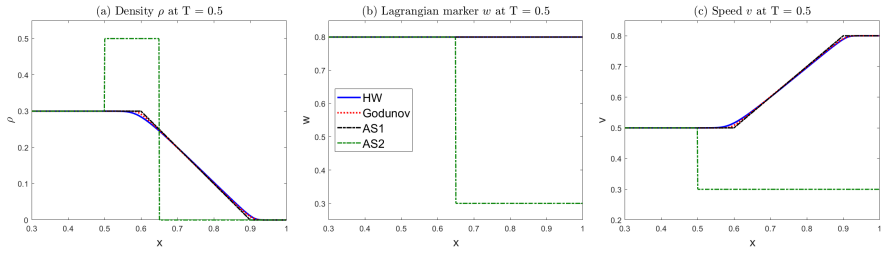

Fig. 7 Test 3 (C) Solutions of the Riemann problem with $(\rho_L, w_L) = (0.3, 0.8)$, $(\rho_R, w_R) = (0, 0.3)$, computed by the Godunov and HW schemes at $T = 0.5$ with $\Delta x = \frac{1}{800}$, compared to the analytical solutions.

- **Test 4:** a Riemann like initial datum with $(\rho_L, w_L) = (0.3, 0.5)$, $(\rho_R, w_R) = (0.7, 0.8)$, whose solution corresponds to a shock followed by a contact discontinuity;
- **Test 5:** a smooth solution corresponding to the initial condition: $\rho(0, x) = 0.45 \exp\left(-\frac{(x-0.5)^2}{2 \cdot 0.1^2}\right) + 0.2$, $w(0, x) = 1.12(x - 0.5)^2 + 0.7$.

We observe that, as expected for first order schemes, the order of convergence is about 0.5 for discontinous solutions and 1 for smooth ones, HW showing in general a slightly higher order than Godunov's, but for bigger errors due to greater viscosity.

Table 1 $\mathbf{L^1}$-error and numerical order of accuracy for the Godunov and HW schemes at $T = 0.5$.

(a) **Test 4**.

	HW		Godunov	
$\frac{1}{\Delta x}$	$\mathbf{L^1}(\Delta x)$	$\gamma(\Delta x)$	$\mathbf{L^1}(\Delta x)$	$\gamma(\Delta x)$
100	$15.37 \cdot 10^{-3}$	-	$13.52 \cdot 10^{-3}$	-
200	$10.66 \cdot 10^{-3}$	0.5283	$9.50 \cdot 10^{-3}$	0.5153
400	$7.32 \cdot 10^{-3}$	0.5427	$6.67 \cdot 10^{-3}$	0.5037
800	$5.02 \cdot 10^{-3}$	0.5439	$4.74 \cdot 10^{-3}$	0.4950
1600	$3.47 \cdot 10^{-3}$	0.5303	$3.37 \cdot 10^{-3}$	0.4898

(b) **Test 5**.

	HW		Godunov	
$\frac{1}{\Delta x}$	$\mathbf{L^1}(\Delta x)$	$\gamma(\Delta x)$	$\mathbf{L^1}(\Delta x)$	$\gamma(\Delta x)$
100	$20.85 \cdot 10^{-3}$	-	$10.25 \cdot 10^{-3}$	-
200	$12.36 \cdot 10^{-3}$	0.7548	$5.37 \cdot 10^{-3}$	0.9320
400	$6.23 \cdot 10^{-3}$	0.9880	$2.76 \cdot 10^{-3}$	0.9631
800	$3.06 \cdot 10^{-3}$	1.0237	$1.37 \cdot 10^{-3}$	1.0091
1600	$1.44 \cdot 10^{-3}$	1.0857	$0.65 \cdot 10^{-3}$	1.0678

4.2 Model calibration: computational cost

In the following section, we compare the computational performance of the proposed HW scheme with the more commonly used Godunov scheme.

We consider real traffic data provided by the Minnesota Department of Transportation (RTMC data) [15]. Thus, we analyse a 5 hours traffic scenario (Friday 02/22/2013, 6am-11am) on a 1.1 km long rampless road stretch equipped with 4

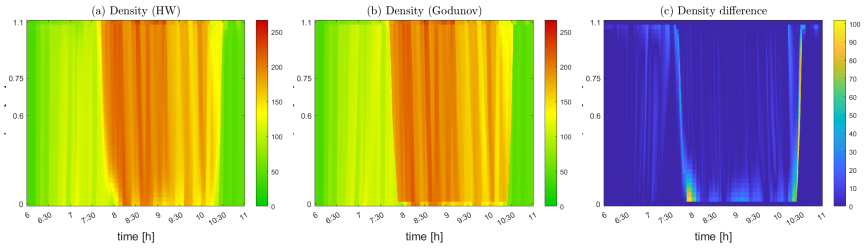

Fig. 8 Space-time density visualization of the simulated data and their difference.

loop detectors which measure the traffic flow and occupancy. For a detailed description and illustration of the traffic scenario, we refer to [18, Section 3].
As in [18], the speed function is given by

$$\mathcal{V}(\rho, w) = w\left(1 - \exp\left(\frac{\mathbf{C}}{\mathbf{V}_{\max}}\left(1 - \frac{\mathbf{R}_{\max}}{\rho}\right)\right)\right),$$

which satisfies (2). The function contains three parameters $\boldsymbol{\theta} = (\mathbf{V}_{\max}, \mathbf{C}, \mathbf{R}_{\max})$ ($\mathbf{V}_{\max}$: maximum speed, $\mathbf{C}$: propagation speed in congestion), which have to be calibrated. In order to compute the optimal parameter set $\boldsymbol{\theta}^*$, we execute a least square optimization which reads as

$$\boldsymbol{\theta}^* = \underset{\boldsymbol{\theta}}{\operatorname{argmin}}\, C(\boldsymbol{\theta}) = \underset{\boldsymbol{\theta}}{\operatorname{argmin}} \sum_{i=1}^{N} \left|q(t_i, x_i) - q^{sim}(t_i, x_i, \boldsymbol{\theta})\right|^2,$$

where N denotes the number of observation points. The quantity of interested is chosen to be the flow, thus $q(t,x)$ (resp. $q^{sim}(t,x)$) denotes the averaged measured (resp. simulated) flow value at time t and loop position x. The optimization is executed in MATLAB by using the global optimization solver `pso` and setting its hybrid function tool to the local `fmincon`-solver. The maximum Lagrangian vehicle property is set to $w_{max} = 140$ and the optimization bounds are the same as in [18, Table 1]. Finally, we compare the calibration parameters, the root-mean square error and the computational time τ between the two numerical schemes in Table 2. We recall that the root-mean square error between an observed traffic quantity y_k and its averaged simulated value y_k^{sim}, for $k \in \{\text{flow, speed, density}\}$, is given by $E^k = \left(\frac{1}{N}\sum_{i=1}^{N} |y_k(t_i, x_i) - y_k^{sim}(t_i, x_i, \boldsymbol{\theta}^*)|^2\right)^{1/2}$. We observe that, for comparable errors and similar calibration parameters, the computational time is reduced by 42% using HW scheme.

Table 2 Calibration parameter, root-mean square error and computational time (in seconds) for the Godunov and HW schemes. RTMC traffic data. In bold: value with a lower error.

	$\mathbf{V}_{\max}$	$\mathbf{C}$	$\mathbf{R}_{\max}$	E^{flow}	E^{speed}	E^{density}	τ
HW	92.23	24.16	442.14	**395.89**	5.66	20.43	298.87
Godunov	94.98	21.39	454.49	396.69	**5.50**	**20.35**	518.34

Acknowledgements This work has been supported by the French government, through the 3IA Côte d'Azur Investments in the Future project managed by the National Research Agency (ANR) with the reference number ANR-19-P3IA-0002. ; the Inria Associated Team "NOLOCO - Efficient numerical schemes for non-local transport phenomena" (2018-2022); the MATH-Amsud 22-MATH-05 "NOTION - NOn-local conservaTION laws for engineering, biological and epidemiological applications: theoretical and numerical" (2022-2023). LMV was partially supported by Centro de Modelamiento Matemático (CMM) FB210005 BASAL funds for centers of excellence from ANID-Chile.

References

1. B. Andreianov, C. Donadello, and M. D. Rosini. A second-order model for vehicular traffics with local point constraints on the flow. *Math. Models Methods Appl. Sci.*, 26(4):751–802, 2016.
2. A. Aw and M. Rascle. Resurrection of "second order" models of traffic flow. *SIAM J. Appl. Math.*, 60(3):916–938, 2000.
3. A. Bressan. *Hyperbolic systems of conservation laws*, volume 20 of *Oxford Lecture Series in Mathematics and its Applications*. Oxford University Press, Oxford, 2000. The one-dimensional Cauchy problem.
4. R. Bürger, A. García, K. H. Karlsen, and J. D. Towers. A family of numerical schemes for kinematic flows with discontinuous flux. *J. Engrg. Math.*, 60(3-4):387–425, 2008.
5. F. A. Chiarello, J. Friedrich, P. Goatin, and S. Göttlich. Micro-macro limit of a nonlocal generalized Aw-Rascle type model. *SIAM J. Appl. Math.*, 80(4):1841–1861, 2020.
6. C. F. Daganzo. The cell transmission model: A dynamic representation of highway traffic consistent with the hydrodynamic theory. *Transportation Research Part B: Methodological*, 28(4):269–287, 1994.
7. S. Fan. *Data-fitted generic second order macroscopic traffic flow models*. PhD thesis, Temple University, 2013.
8. S. Fan, M. Herty, and B. Seibold. Comparative model accuracy of a data-fitted generalized Aw-Rascle-Zhang model. *Netw. Heterog. Media*, 9(2):239–268, 2014.
9. P. Goatin and A. Würth. The initial boundary value problem for second order traffic flow models with vacuum: existence of entropy weak solutions. Preprint, Oct. 2022.
10. S. K. Godunov. A difference method for numerical calculation of discontinuous solutions of the equations of hydrodynamics. *Mat. Sb. (N.S.)*, 47 (89):271–306, 1959.
11. M. Hilliges and W. Weidlich. A phenomenological model for dynamic traffic flow in networks. *Transportation Research Part B: Methodological*, 29(6):407–431, 1995.
12. J.-P. Lebacque, H. Haj-Salem, and S. Mammar. Second order traffic flow modeling: supply-demand analysis of the inhomogeneous Riemann problem and of boundary conditions. *Proceedings of the 10th Euro Working Group on Transportation (EWGT)*, 3(3), 2005.
13. J.-P. Lebacque, S. Mammar, and H. H. Salem. Generic second order traffic flow modelling. In *Transportation and Traffic Theory 2007*, 2007.
14. M. J. Lighthill and G. B. Whitham. On kinematic waves. II. A theory of traffic flow on long crowded roads. *Proc. Roy. Soc. London Ser. A*, 229:317–345, 1955.
15. Minnesota Departement of Transportation. Mn/Dot Traffic Data. Website: http://data.dot.state.mn.us/datatools/.
16. P. I. Richards. Shock waves on the highway. *Operations Res.*, 4:42–51, 1956.
17. B. Temple. Systems of conservation laws with invariant submanifolds. *Trans. Amer. Math. Soc.*, 280(2):781–795, 1983.
18. A. Würth, M. Binois, P. Goatin, and S. Göttlich. Data-driven uncertainty quantification in macroscopic traffic flow models. *Advances in Computational Mathematics*, 48(6):1–26, 2022.
19. H. M. Zhang. A non-equilibrium traffic model devoid of gas-like behavior. *Transportation Res. Part B*, 36(3):275–290, 2002.